AIP Advances

Determination of dynamic shear strength of 2024 aluminum alloy under shock compression

H. S. Zhang, M. Yan, H. Y. Wang, L. T. Shen, and L. H. Dai

Citation: AIP Advances **6**, 045309 (2016); doi: 10.1063/1.4947136
View online: http://dx.doi.org/10.1063/1.4947136
View Table of Contents: http://scitation.aip.org/content/aip/journal/adva/6/4?ver=pdfcov
Published by the AIP Publishing

Determination of dynamic shear strength of 2024 aluminum alloy under shock compression

H. S. Zhang,[1,2] M. Yan,[1] H. Y. Wang,[1] L. T. Shen,[1] and L. H. Dai[1,a]
[1]*State Key Laboratory of Nonlinear Mechanics, Institute of Mechanics, Chinese Academy of Sciences, Beijing 100190, China*
[2]*State Key Laboratory of Explosion Science and Technology, Beijing Institute of Technology, Beijing 100081, China*

(Received 11 February 2016; accepted 7 April 2016; published online 14 April 2016)

A series of plate impact shock-reshock and shock-release experiments were conducted by using an one-stage light gas gun to determine the critical shear strength of the 2024 aluminum alloy under shock compression levels ranging from 0.66 to 3.05 GPa in the present study. In the experiments, a dual flyer plate assembly, i.e., the 2024 aluminum alloy flyer backed either by a brass plate or a PMMA plate, was utilized to produce reshock or release wave. The stress profiles of uniaxial plane strain wave propagation in the 2024 aluminum alloy sample under different pre-compressed states were measured by the embedded stress gauges. The stress-strain data at corresponding states were then calculated by a Lagrangian analysis method named as path line method. The critical shear strengths at different stress levels were finally obtained by self-consistent method. The results show that, at the low shock compression level (0.66 to 3.05 GPa), the critical shear strength of the 2024 aluminum alloy cannot be ignored and increases with the increasing longitudinal stress, which may be attributed to rate-dependence and/or pressure dependent yield behavior of the 2024 aluminum alloy. [http://dx.doi.org/10.1063/1.4947136]

I. INTRODUCTION

The 2024 aluminum alloy is extensively used in aeronautics and astronautics area, defense utility, civil industry because of its excellent properties, such as low density, high strength and good ductility.[1] It is very important to study the constitutive response of the 2024 aluminum alloy under shock compression.

It is often assumed that the one-dimension strain compression curve is consistent with hydrostatic compression curve, if the shock pressure is up to eight times the Hugoniot elastic limit. In this case, the material can be treated as liquid, thus the hydrodynamic model can be used to characterize the high-pressure response of the materials.[2] In fact, when the materials deforms from elastic state to plastic state, and the hydrostatic state, the material is undergoing not only the normal stresses, but also inevitably the shear stresses in this process. However in conventional shock-wave experiments only the longitudinal stress is measured. It is true that the longitudinal stress is used to deduce the equation of state in thermodynamic equilibrium state when the materials are compressed with high-pressure shock wave. However, it can't accurately characterize the response of the material in the middle-pressure and low-pressure shock levels. Hence it is necessary to determine the critical shear strength of the materials at the low and/or middle pressure range.

The critical shear strength under shock wave can be obtained by directly measuring the lateral stress or self-consistent technique.[3] Piezoresistive gauges have been utilized for several decades to measure the lateral stress in shock loaded solids.[4] This technique was first used by Bernstein et al.,[5]

[a]Email address: lhdai@lnm.imech.ac.cn

with manganin wires embedded in steel specimens along the longitudinal and lateral orientations. In the following years, the piezoresistive stress gauge (made of manganin or ytterbium) technique was also used as lateral stress transducers by Rosenberg et al.,[6,7] Gupta et al.,[8,9] Dai et al.,[10] Winter et al.[11] The calibration of the gauge is the focus of their researches. Since the lateral stresses in the shock-loaded solids are usually unknown, a simple calibration of lateral gauges, in terms of resistance changes vs. lateral stresses is practically impossible to achieve.[4] The calibration of the lateral gauge depends on the longitudinal stress in the embedding matrix and the strength of the gauge. So the accuracy of the gauge's strength will strongly affect the experimental results. For example, Rosenberg et al.[4] found that the new values for the gauge's strength are about half the corresponding value from the Ref. 12 through a simplified analysis. In view of the fact that the calibration of lateral gauge is uncertainty, self-consistent technique[13–17] was used in the present study to determine the shear strength of 2024 aluminum alloy since it has advantages over the lateral stress gauge technique.

In this paper, to determine the critical strength of 2024 aluminum alloy, a series of shock-reshock and shock-release experiments were conducted with a dual flyer plate assembly on an one-stage light gas gun. And then the stress profiles of one-dimension plane strain wave propagation in 2024 aluminum alloy specimens under different preshocked states were measured. The stress-strain data at corresponding states were determined by Lagrangian analysis method. Finally, the critical shear strengths at different stress levels were obtained by self-consistent method.

In section II, the material used in present study is introduced. In section III, the configuration of shock-reshock and shock-release experiments is presented. In section IV, the basic approach of the self-consistent technique is described. In section V, the Lagrangian analysis method is introduced and the calculation procedure is described. In section VI, the experimental results are given, the stress-strain data are deduced from the wave profiles through the path line method, and the shear strengths in different stress level are obtained by self-consistent method. Finally, the conclusions are summarized in Section VII.

II. MATERIAL

The materials used in the present study were 2024 aluminum alloys, whose chemical compositions are given in Table I. This materials were supplied as an extruded bar, which was manufactured using cold working followed by natural aging (T4). The microstructure of etched longitudinal sections of the alloy is shown in Fig. 1. As shown in Fig. 1, the $CuMgAl_2$ precipitate phase distributes uniformly in the grain interior, with the grains extruded as a narrow strip.

III. SHOCK-RESHOCK AND SHOCK-RELEASE EXPERIMENTS

The shock-reshock and shock-release experiments were conducted by one-stage light gas gun at the Institute of Mechanics, Chinese Academy of Sciences. The diameter and the length of the barrel for the gun is 101 mm and 17m, respectively. The projectile velocity which can be achieved by the gun is ranging from 20 m/s to 1400 m/s and its error can be controlled to be less than five percent. The tilt is less than 10^{-3} radians. Fig. 2 shows the configuration of these experiments. A dual flyer assembly was used. The 2024 aluminum alloy flyer was backed either by a brass plate to produce reshock wave or by a PMMA plate to produce release wave. In all of the experiments, the 2024 aluminum flyer and backing plate were 75 mm diameter disks, and the 2024 aluminum targets were 70 mm diameter disks. To investigate the propagation of the stress wave, the stress gauges are

TABLE I. Chemical composition of the tested alloys (mass%).

Cu	Mg	Mn	Fe	Si	Zn	Ti
4.26	1.48	0.52	0.24	0.16	0.04	0.04

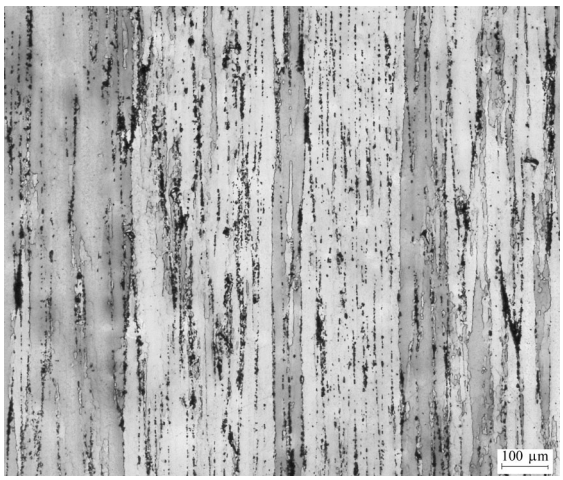

FIG. 1. Microstructure of etched 2024-T4 aluminum alloy (longitudinal section).

embedded in the target plates. Under shock wave, the gauges are compressed with movement of the particle of the materials, so they can record the histories of stress in these sites.

In the present study, four preshocked states were selected and two experiments were conducted for each preshocked states. The parameters for those experiments are listed in Table II and Table III.

IV. SELF-CONSISTENT TECHNIQUE

Fowls et al.[18] proposed that the shear strength of the material under high pressure shock can be determined by comparing the measured longitudinal stress with the data of hydrostatic pressure experiments. However, a predetermined hydrostatic curve was required in his method. In the 1970s to 1980s, Asay, Lipkin and Chhabidas[13–15] proposed and developed the self-consistent method to measure the shear strength under shock compression. This method estimates the yield strength of the materials under shock pressure by utilizing shock-reshock and shock-release experimental data from a pre-compressed state. Its principle is described as follows.

High-strain-rate uniaxial strain condition can be achieved during plate impact experiments. For the isotropic materials, the longitudinal stress σ_x, the lateral stress σ_y and σ_z (equal to σ_y in

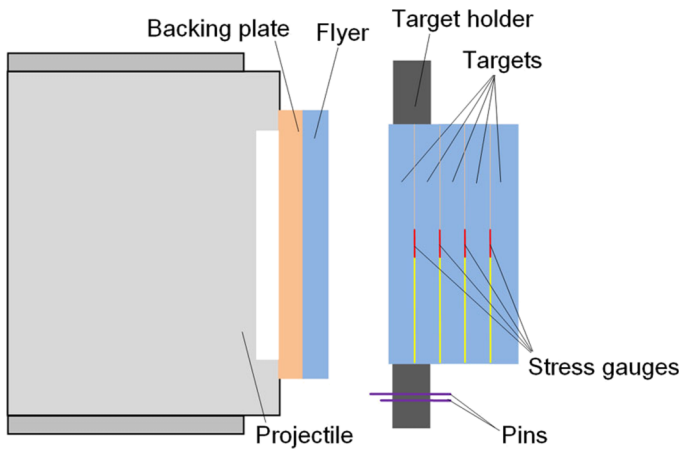

FIG. 2. Experimental configuration of shock-reshock and shock-release experiments.

TABLE II. Parameters for shock-reshock experiments.

		Flyer thickness (mm)		Target thickness (mm)				
Shot Number	Impact velocity (m/s)	2024Al	Brass	δ1	δ2	δ3	δ4	δ5
04-24	96.4	3.12	2.08	3.00	4.12	4.10	4.10	15.04
04-25	197.8	3.06	2.12	3.00	4.06	4.02	3.98	15.12
04-31	312.3	3.20	1.96	3.08	4.08	4.04	4.00	15.08
04-33	390.8	3.22	2.02	3.12	4.12	4.00	4.02	14.92

uniaxial strain condition), and the mean stress $\overline{\sigma}$ have the following relationship:

$$\overline{\sigma} = \frac{1}{3}\left(\sigma_x + 2\sigma_y\right). \tag{1}$$

For plastic response under uniaxial strain, either von Mises or Tresca criterion leads to the following relation:

$$\sigma_x - \sigma_y = \pm 2\tau, \tag{2}$$

where τ is the shear stress. Thus, in the yield surface the following relation between the longitudinal stress and the mean stress can be obtained:

$$\sigma_x = \overline{\sigma} \pm \frac{4}{3}\tau. \tag{3}$$

So, for perfectly plastic response, the plastic portions of the reshock and release paths are parallel to the hydrostat curve.

However, only a few materials exhibit such simple response under uniaxial strain shock loading. It is necessary to modify the above-mentioned model to describe broader class of materials. The kinematic hardening model can describe the behavior such as anisotropic effect. The important characteristic of the kinematic hardening model is the yield locus can translate with the plastic deformation. Assuming that the symmetry axis of the yield surface remains parallel to the hydrostat during the deformation, Eq. (3) can be rewritten to following equations:

$$(\sigma_x - \overline{\sigma}) - \alpha_x = \pm\frac{4}{3}\tau, \tag{4}$$

Where, α_x is the x displacement of the symmetry axis of the yield surface from the hydrostat.

Fig. 3 illustrates how to determine the shear strength and the mean stress from reshock and release data. It is assumed that the material has been preshocked to the σ_{x1} state. States 2 and 4 are defined as maximum or minimum shear stress states at the reshock path or the release path because the Lagrangian wave velocity reduces to the bulk wave speed at those states. Once states σ_{x2} and σ_{x4} are determined, the maximum stress $\sigma_x(A)$ and the minimum stress $\sigma_x(B)$ at the preshocked

TABLE III. Parameters for shock-release experiments.

		Flyer thickness (mm)		Target thickness (mm)				
Shot Number	Impact velocity (m/s)	2024Al	PMMA	δ1	δ2	δ3	δ4	δ5
04-22	99.7	3.22	2.98	3.14	3.88	3.92	3.88	15.04
04-23	200.4	3.20	3.02	3.06	4.10	3.98	4.02	15.10
04-27	301.5	3.10	3.18	2.96	4.02	4.10	4.08	14.98
04-30	391.5	3.12	3.06	3.02	4.04	4.08	4.12	15.20

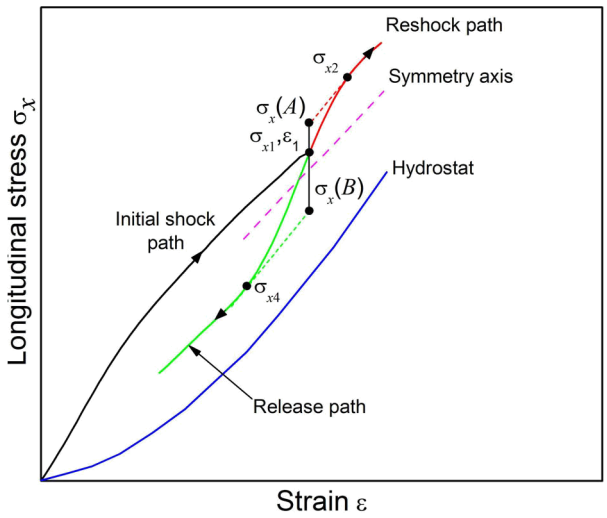

FIG. 3. Longitudinal stress versus strain for kinematic hardening material under preshocked state.

state can be calculated graphically. Since

$$(\sigma_x(A) - \overline{\sigma}) - \alpha_x = \frac{4}{3}\tau_c, \tag{5}$$

$$(\sigma_x(B) - \overline{\sigma}) - \alpha_x = -\frac{4}{3}\tau_c, \tag{6}$$

the following equation can be obtained:

$$\tau_c = \frac{3}{8}(\sigma_x(A) - \sigma_x(B)), \tag{7}$$

Eq. (7) can be used to obtain the critical shear strength at the current preshocked state.

The following assumptions should be made when applying the self-consistent method to real-materials: (i) reshock and release from the preshocked state are rate independent, (ii) a yield surface exists for the materials after shocking which can be experimentally detected as a transition from quasi-elastic to plastic response, (iii) the yield surface remains symmetric although it may translate in stress space during shock loading, (iv) the yield surface has an axis of symmetry which remains parallel to the hydrostatic curve during deformation.

V. LAGRANGIAN ANALYSIS METHOD

Under shock wave, the inertia effect of the materials is usually coupled with the strain rate effect. The constitutive model of the materials under high strain rate depends on the analysis of the attenuating waves in the materials. The information of one-dimension plane strain wave propagation in the materials is generally obtained by plate impact experiment.

Lagrangian analysis method can deduce the stress-strain relation for the materials from the uniaxial plane strain waves measured by the gauges. This method was proposed by Fowles, Cowperthwaite and Williams[19,20] in the 1970s. The passage of the disturbance is recorded by embedding the stress or particle velocity gauges in different Lagrangian positions in the sample. Then the histories of the unknown mechanical parameters (such as particle velocity, stress, density, strain and internal energy) can be obtained through several universal conservation equations.

The path line method is a common method in Lagrangian analysis. This method was proposed by Grady[21] in 1973. Soon afterwards, Seaman[22] proposed the curve fitting method based on the Grady's method. From then on this method has been used by several researchers.[23–25] The principle of the path line method is given as follows.

Under one-dimension strain, the flow of the particle follows the conservation laws of mass, momentum and energy.

$$\text{Mass conservation: } \left(\frac{\partial \varepsilon}{\partial t}\right)_h + \left(\frac{\partial u}{\partial h}\right)_t = 0, \tag{8}$$

$$\text{Momentum conservation: } \left(\frac{\partial u}{\partial t}\right)_h + \frac{1}{\rho_0}\left(\frac{\partial \sigma}{\partial h}\right)_t = 0, \tag{9}$$

$$\text{Energy conservation: } \left(\frac{\partial E}{\partial t}\right)_h + \frac{\sigma}{\rho_0}\left(\frac{\partial u}{\partial h}\right)_t = 0, \tag{10}$$

where u is the particle velocity, ε is the strain, h is the Lagrangian spatial coordinate, E is the specific internal energy, ρ_0 is the initial density, σ is the stress in the direction of propagation.

To determine the histories of the strain, the particle velocity and the specific internal energy of each gauge, Eqs. (8)-(10)) must be integrated along the experimental record lines. The integrated forms can be written as follows:

$$\varepsilon_2 = \varepsilon_1 - \int_{t_1}^{t_2} \left(\frac{\partial u}{\partial h}\right)_t dt, \tag{11}$$

$$u_2 = u_1 - \frac{1}{\rho_0}\int_{t_1}^{t_2} \left(\frac{\partial \sigma}{\partial h}\right)_t dt, \tag{12}$$

$$E_2 = E_1 - \frac{\sigma}{\rho_0}\int_{t_1}^{t_2} \left(\frac{\partial u}{\partial h}\right)_t dt. \tag{13}$$

The path line method is illustrated in Fig. 4. This method divides the gauge records into discrete time intervals, and connects the records in such way that the lines are approximately in the directions of wave propagation. These lines connect the peaks of the records and other points with similar features.

Generally, the mechanical parameter in the flow field has the following relationship along the path line:

$$\left(\frac{\partial \varphi}{\partial h}\right)_t = \frac{d\varphi}{dh} - \left(\frac{\partial \varphi}{\partial t}\right)_h \frac{dt}{dh}, \tag{14}$$

where φ may denote stress σ, particle velocity u, or specific internal energy E.

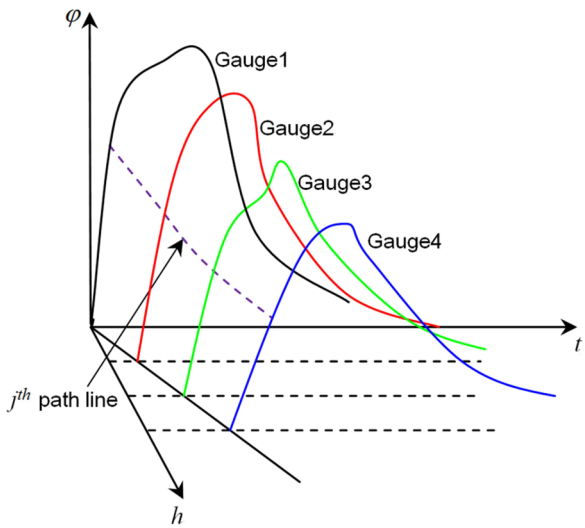

FIG. 4. Gauge record lines and path lines in φ-h-t space.

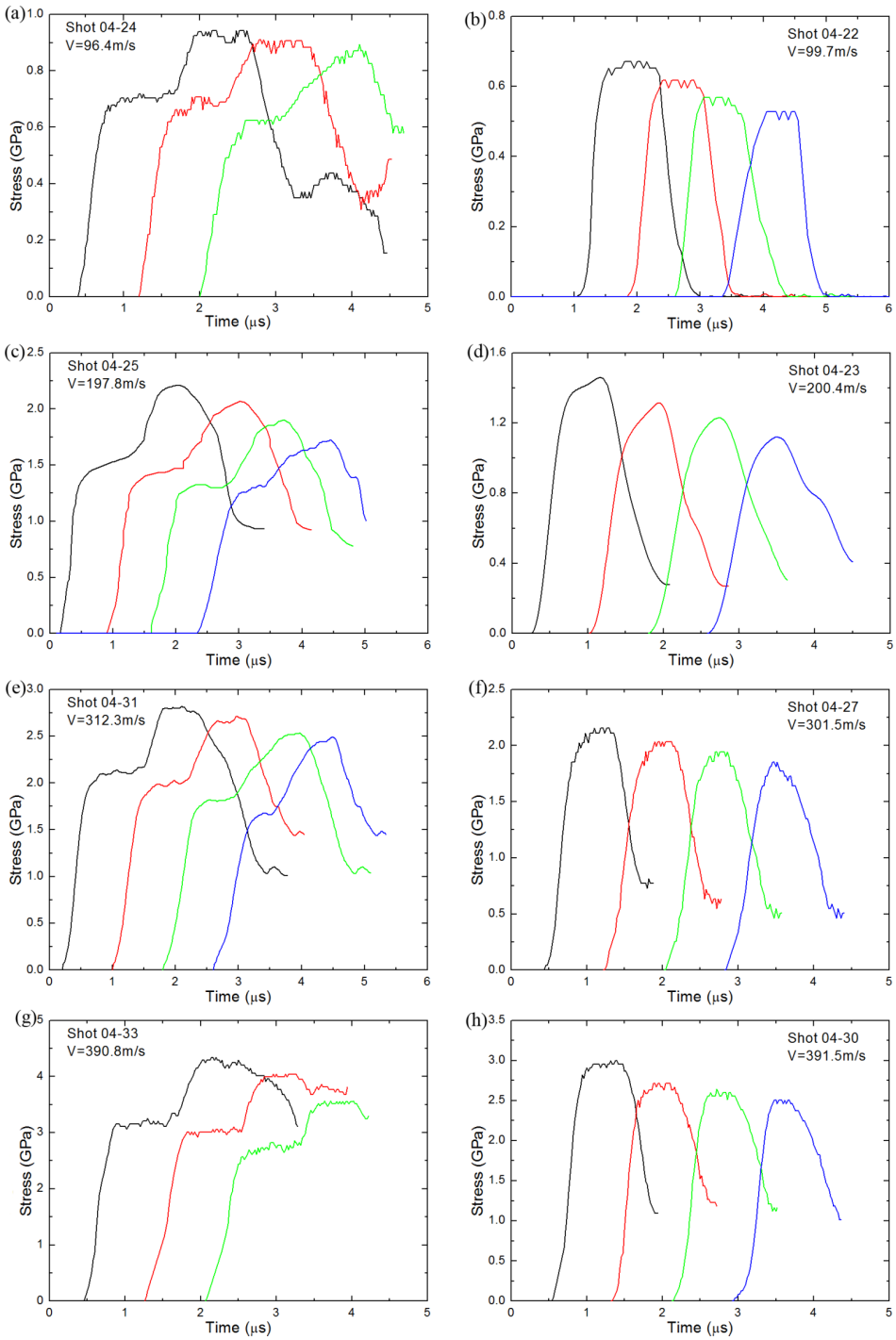

FIG. 5. Stress profiles of shock-reshock and shock-release under different preshocked states obtained from the multiple gauges.

Along the path line, the Eqs. (11)-(13) can be written as follows:

$$\varepsilon_{j+1,k} = \varepsilon_{j,k} - \frac{1}{2}\left(\frac{du_{j+1,k}}{dh} - \frac{\partial u_{j+1,k}}{\partial t}\cdot\frac{dt_{j+1,k}}{dh} + \frac{du_{j,k}}{dh} - \frac{\partial u_{j,k}}{\partial t}\cdot\frac{dt_{j,k}}{dh}\right)\cdot\left(t_{j+1,k} - t_{j,k}\right), \tag{15}$$

$$u_{j+1,k} = u_{j,k} - \frac{1}{2\rho_0}\left(\frac{d\sigma_{j+1,k}}{dh} - \frac{\partial \sigma_{j+1,k}}{\partial t}\cdot\frac{dt_{j+1,k}}{dh} + \frac{d\sigma_{j,k}}{dh} - \frac{\partial \sigma_{j,k}}{\partial t}\cdot\frac{dt_{j,k}}{dh}\right)\cdot\left(t_{j+1,k} - t_{j,k}\right), \tag{16}$$

$$E_{j+1,k} = E_{j,k} - \frac{\sigma_{j+1,k} + \sigma_{j,k}}{4\rho_0}\left(\frac{du_{j+1,k}}{dh} - \frac{\partial u_{j+1,k}}{\partial t}\cdot\frac{dt_{j+1,k}}{dh} + \frac{du_{j,k}}{dh} - \frac{\partial u_{j,k}}{\partial t}\cdot\frac{dt_{j,k}}{dh}\right) \cdot \left(t_{j+1,k} - t_{j,k}\right). \quad (17)$$

If the gauges record the histories of the stress, the particle velocity fields can be derived from the equation (16). Then strain and the specific internal energy can be obtained from the equation (15) and the equation (17), respectively. Finally the stress-strain relationship can be obtained.

VI. EXPERIMENTAL RESULTS AND DISCUSSION

The stress profiles under different impact velocities obtained from multiple stress gauges are showed in Fig. 5. The stress-strain data of the 2024 aluminum alloy under the corresponding preshocked states were calculated through the path line method.

Fig. 6 illustrates the calculation of the critical shear strength of the 2024 aluminum alloy under different preshocked states by self-consistent method. The critical shear strength can be obtained by following four steps:[16,26] (i) State 2 and state 4 are defined as maximum or minimum shear stress states at the reshock path or the release path because the Lagrangian wave velocity reduces to the bulk wave speed at those states; (ii) A tangent line can be drawn at the state 2 or state 4, and the extension of the tangent line can be made; (iii) The maximum stress point A or the minimum stress point B can be determined by the intersection point between the extending line and the vertical line passing the preshocked point; (iv) Finally, the critical shear strengths can be calculated by equation (7).

The values calculated by above steps are listed in Table IV. The critical shear strengths at different stress levels are plotted in Fig. 7. It is shown that the critical shear strength increases with

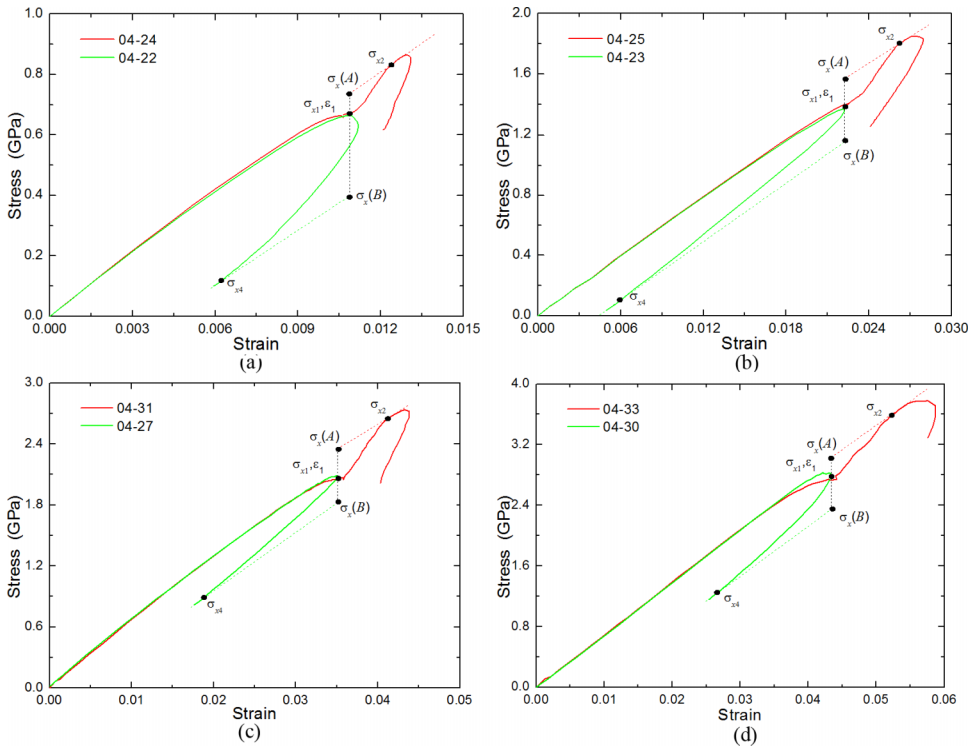

FIG. 6. Stress-strain curves under the corresponding preshocked states calculated from the attenuation experiments: (a) Impact velocity about 100m/s; (b) Impact velocity about 200m/s; (c) Impact velocity about 300m/s; and (d) Impact velocity about 400m/s.

TABLE IV. Results calculated by self-consistent method.

Longitudinal stress σ_x (GPa)	Maximums tress $\sigma_x(A)$ (GPa)	Minimum stress $\sigma_x(B)$ (GPa)	Critical shear stress τ_c (GPa)	Ratio τ_c/σ_x
0.67	0.74	0.40	0.128	19.1%
1.38	1.57	1.15	0.158	11.4%
2.07	2.35	1.82	0.199	9.6%
2.79	3.03	2.34	0.258	9.2%

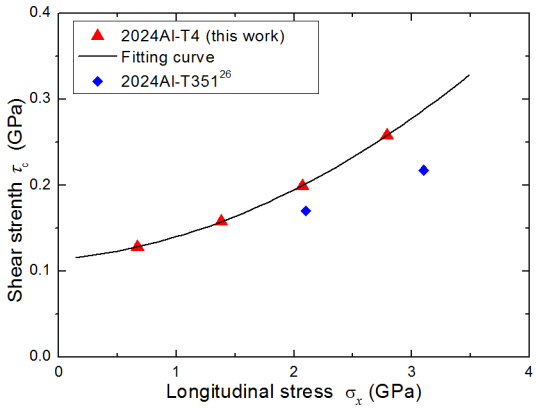

FIG. 7. Critical shear strengths in different stress levels.

the increasing longitudinal stress. The critical shear strength increases from 0.128 to 0.258 GPa when the longitudinal stress increases from 0.67 to 2.79 GPa. But the ratio of the critical shear strength to the longitudinal stress decreases and tends to be constant value with the increasing longitudinal stress. Our results have also been compared with the data from previous research,[27] where the dynamic shear strengths of 2024- T351 Aluminum at different shock stress levels have been inferred from the cusp in the release curve. As shown in Fig. 7, our values are close to the values of Ref. 27. The difference partly is due to the different treat state of the materials.

The critical shear strength as the function of the longitudinal stress can be fitted as:

$$\tau_c = 0.113 + .0.012\sigma_x + 0.014\sigma_x^2, \tag{18}$$

Huang[28] has similar results in measuring the strengths of five aluminum materials (including 6061 aluminum alloy with three average grain sizes, pure aluminum and ultrapure aluminum) for shock compression over the stress range of 4–22 GPa. It is envisioned that multiple factors, including rate and pressure dependences of the flow behaviors for the 2024 aluminum alloy, are collectively responsible for the increasing critical shear strength with increasing impact stress.

VII. CONCLUSION

In this paper, shock-reshock and shock-release experiments of the 2024 aluminum alloy were performed using a dual flyer assembly with an one-stage light gas gun. The stress profiles in 2024 aluminum alloy targets under different preshocked states were recorded. The stress-strain curves at the corresponding states were analyzed with path line method. The shear strengths in different stress levels were obtained by self-consistent method. The results show that the shear strength of material cannot be ignored and it increases with the longitudinal stress under the low stress shock. In the end the relation between the critical shear strength and the longitudinal stress was also obtained. It is envisioned that multiple factors, including rate and pressure dependence of the flow behaviors for the 2024 aluminum alloy, are collectively responsible for the increasing critical shear strength with increasing impact stress.

ACKNOWLEDGMENT

This work was financially supported by the National Nature Science Foundation of China (Grant No. 10232040 11132011 and 11472288). The authors thank Prof. Y.L.Deng for the assistance in experiments of light gas gun, and the assistance of Prof. F.P.Yuan in analysis techniques is gratefully acknowledged.

[1] J. A. Rodríguez-Martínez, A. Rusinek, and A. Arias, Thin. Struc. **49**, 819 (2011).
[2] F. Q. Jing, *Introduction to Experimental Equation of State* (Academic, Beijing, 1977), p. 65.
[3] T. J. Vogler and L. C. Chhabildas, Int. J. Impact Eng. **33**, 812 (2006).
[4] Z. Rosenberg and G. Moshel, J. Appl. Phys. **115**, 103511 (2014).
[5] D. Bernstein, C. Godfrey, A. Klein, and W. Shimin, *Behavior of Dense Media Under High Dynamic Pressures* (Gordon and Bresch, New York, 1968), p. 461.
[6] Z. Rosenberg, Y. Partom, and D. Yaziv, J. Appl. Phys. **52**, 755 (1981).
[7] Z. Rosenberg and Y. Partom, J. Appl. Phys. **58**, 3072 (1985).
[8] Y. M. Gupta, D. D. Keough, D. Henley, and D. F. Walter, Appl. Phys. Lett. **37**, 395 (1980).
[9] Y. M. Gupta, J. Appl. Phys. **54**, 6256 (1983).
[10] L. H. Dai, M. Yan, and L. T. Shen, Chin. Phys. Lett. **21**, 707 (2004).
[11] R. E. Winter and E. J. Harris, J. Phys. D:Appl. Phys. **39**, 5323 (2006).
[12] Z. Rosenberg and Y. Partom, J. Appl. Phys. **57**, 5084 (1985).
[13] J. R. Asay and J. J. Lipkin, J. Appl. Phys. **49**, 4242 (1978).
[14] J. R. Asay and L. C. Chhabildas, J. Appl. Phys. **51**, 4774 (1980).
[15] J. R. Asay and L. C. Chhabildas, SAND88-0306, 1988.
[16] F. Yuan, L. Tsai, V. Prakash, D.P. Dandekar, and A.M. Rajendran, J. Appl. Phys. **103**, 103537 (2008).
[17] R. Fowles, J. Appl. Phys. **32**, 1475 (1961).
[18] J. B. Hu, C. D. Dai, Y. Y. Yu, and H. Tan, Explo. and Shock Waves. **26**, 516 (2006).
[19] R. Fowles and R. F. Williams, J. Appl. Phys. **41**, 360 (1970).
[20] M. Cowperthwaite and R. F. Williams, J. Appl. Phys. **42**, 456 (1971).
[21] D. E. Grady, J. Geop. Res. **78**, 1299 (1973).
[22] L. Seaman, J. Appl. Phys. **45**, 4303 (1974).
[23] H. F. Liu and J. G. Ning, Mech. of Mater. **41**, 1298 (2009).
[24] L. Wang, J. Zhu, and H. Lai, Strain **47**, 173 (2011).
[25] W. J. Tao and S. Huan, Acta.Phys. Sin. **6**, 200793 (2012).
[26] W. D. Reinhart and L. C. Chhabildas, Int. J. Impact Eng. **29**, 601 (2003).
[27] Z. Rosenberg, Y. Partom, and D. Yaziv, J. Appl. Phys. **56**, 143 (1984).
[28] H. Huang and J. R. Asay, J. Appl. Phys. **98**, 033524 (2005).